

Single-molecule orientation determination with multiview polarized illumination: modeling and microscope design

TALON CHANDLER,^{1,*} SHALIN MEHTA,² HARI SHROFF,^{3,4} RUDOLF OLDENBOURG,^{2, 5} AND PATRICK J. LA RIVIÈRE^{1, 4}

¹*University of Chicago, Department of Radiology, Chicago, Illinois 60637, USA*

²*Marine Biological Laboratory, Bell Center for Regenerative Medicine, Woods Hole, Massachusetts, USA*

³*Section on High Resolution Optical Imaging, National Institute of Biomedical Imaging and Bioengineering, National Institutes of Health, Bethesda, Maryland 20892, USA*

⁴*Whitman Center, Marine Biological Laboratory, Woods Hole, Massachusetts 02543, USA*

⁵*Brown University, Department of Physics, Providence, Rhode Island 02912, USA*

*talonchandler@talonchandler.com

Abstract: We investigate the use of polarized illumination in multiview microscopes for determining the orientation of single molecules. First, we relate the orientation of single molecules to measurable intensities in multiview microscopes and develop an information theoretic metric—the solid angle uncertainty—to compare the ability of multiview microscopes to estimate the orientation of single molecules. Next, we compare a broad class of microscopes using this metric—single- and dual-view microscopes with varying illumination polarization, illumination numerical aperture (NA), detection NA, obliquity, asymmetry, and exposure. We find that multiview microscopes are better at determining the orientation of single molecules than single-view microscopes. We also find that choosing a small illumination NA and a large detection NA are good design choices, that multiview widefield microscopes can benefit from oblique illumination and detection, and that asymmetric NA microscopes can benefit from exposure asymmetry.

OCIS codes: (110.0110) Imaging systems; (180.2520) Fluorescence microscopy; (180.0180) Microscopy; (180.6900) Three-dimensional microscopy; (130.5440) Polarization-selective devices; (260.5430) Polarization.

References and links

1. E. J. Peterman, H. Sosa, L. S. Goldstein, and W. E. Moerner, “Polarized fluorescence microscopy of individual and many kinesin motors bound to axonemal microtubules,” *Biophys. J.* **81**, 2851–2863 (2001).
2. J. N. Forkey, M. E. Quinlan, M. A. Shaw, J. E. T. Corrie, and Y. E. Goldman, “Three-dimensional structural dynamics of myosin V by single-molecule fluorescence polarization,” *Nature* **422**, 399–404 (2003).
3. A. S. Backer, M. Lee, and W. E. Moerner, “Enhanced DNA imaging using super-resolution microscopy and simultaneous single-molecule orientation measurements,” in “Conference on Lasers and Electro-Optics,” (Optical Society of America, 2016), p. JTh4B.4.
4. S. B. Mehta, M. McQuilken, P. J. La Rivière, P. Occhipinti, A. Verma, R. Oldenbourg, A. S. Gladfelter, and T. Tani, “Dissection of molecular assembly dynamics by tracking orientation and position of single molecules in live cells,” *Proc. Natl. Acad. Sci. U.S.A.* **113**, E6352–E6361 (2016).
5. B. DeMay, N. Noda, A. Gladfelter, and R. Oldenbourg, “Rapid and quantitative imaging of excitation polarized fluorescence reveals ordered septin dynamics in live yeast,” *Biophys. J.* **101**, 985–994 (2011).
6. M. McQuilken, M. S. Jentzsch, A. Verma, S. B. Mehta, R. Oldenbourg, and A. S. Gladfelter, “Analysis of septin reorganization at cytokinesis using polarized fluorescence microscopy,” *Front. Cell Dev. Biol.* **5**, 42 (2017).
7. A. Anantharam, B. Onoa, R. H. Edwards, R. W. Holz, and D. Axelrod, “Localized topological changes of the plasma membrane upon exocytosis visualized by polarized tifrm,” *J. Cell Biol.* **188**, 415–428 (2010).
8. M. P. Backlund, M. D. Lew, A. S. Backer, S. J. Sahl, and W. E. Moerner, “The role of molecular dipole orientation in single-molecule fluorescence microscopy and implications for super-resolution imaging,” *ChemPhysChem* **15**, 587–599 (2014).
9. M. A. Lieb, J. M. Zavislán, and L. Novotny, “Single-molecule orientations determined by direct emission pattern imaging,” *J. Opt. Soc. Am. B* **21**, 1210–1215 (2004).
10. A. S. Backer and W. E. Moerner, “Extending single-molecule microscopy using optical Fourier processing,” *J. Phys. Chem. B* **118**, 8313–8329 (2014).

11. A. Agrawal, S. Quirin, G. Grover, and R. Piestun, “Limits of 3D dipole localization and orientation estimation for single-molecule imaging: towards Green’s tensor engineering,” *Opt. Express* **20**, 26667–26680 (2012).
12. A. Débarre, R. Jaffiol, C. Julien, D. Nutarelli, A. Richard, P. Tchénio, F. Chaput, and J.-P. Boilot, “Quantitative determination of the 3D dipole orientation of single molecules,” *Eur. Phys. J. D.* **28**, 67–77 (2004).
13. R. Oldenbourg and G. Mei, “New polarized light microscope with precision universal compensator,” *J. Microsc.* **180**, 140–147 (1995).
14. J. T. Fourkas, “Rapid determination of the three-dimensional orientation of single molecules,” *Opt. Lett.* **26**, 211–213 (2001).
15. C.-Y. Lu and D. A. V. Bout, “Analysis of orientational dynamics of single fluorophore trajectories from three-angle polarization experiments,” *J. Chem. Phys.* **128**, 244501 (2008).
16. Y. Wu, P. Wawrzusin, J. Senseney, R. S. Fischer, R. Christensen, A. Santella, A. G. York, P. W. Winter, C. M. Waterman, Z. Bao, D. A. Colon-Ramos, M. McAuliffe, and H. Shroff, “Spatially isotropic four-dimensional imaging with dual-view plane illumination microscopy,” *Nat. Biotechnol.* **31**, 1032–1038 (2013).
17. R. K. Chhetri, F. Amat, Y. Wan, B. Hockendorf, W. C. Lemon, and P. J. Keller, “Whole-animal functional and developmental imaging with isotropic spatial resolution,” *Nat. Methods* **12**, 1171–1178 (2015).
18. Y. Wu, P. Chandris, P. W. Winter, E. Y. Kim, V. Jaumouillé, A. Kumar, M. Guo, J. M. Leung, C. Smith, I. Rey-Suarez, H. Liu, C. M. Waterman, K. S. Ramamurthi, P. J. La Rivière, and H. Shroff, “Simultaneous multiview capture and fusion improves spatial resolution in wide-field and light-sheet microscopy,” *Optica* **3**, 897–910 (2016).
19. Y. Wu, A. Kumar, C. Smith, E. Ardiel, P. Chandris, R. Christensen, I. Rey-Suarez, M. Guo, H. Vishwasrao, J. Chen, J. Tang, A. Upadhyaya, P. La Rivière, and H. Shroff, “Reflective imaging improves resolution, speed, and collection efficiency in light sheet microscopy,” *bioRxiv* (2017).
20. S. M. Kay, *Fundamentals of statistical signal processing* (Prentice Hall PTR, 1993).
21. T. W. Anderson, *An introduction to multivariate statistical analysis* (Wiley New York, 1958).
22. L. Novotny and B. Hecht, *Principles of Nano-Optics* (Cambridge University Press, 2006).
23. M. Levoy, R. Ng, A. Adams, M. Footer, and M. Horowitz, “Light field microscopy,” in “ACM SIGGRAPH 2006 Papers,” (ACM, New York, NY, USA, 2006), SIGGRAPH ’06, pp. 924–934.

1. Introduction

The orientation of single molecules is a valuable reporter for biological processes. By imaging biological samples with fluorescent probes that are fixed to known structures, researchers have studied the dynamics of motor proteins [1,2], DNA [3], actin [4], septin [5,6], and membranes [7]. The number of techniques available to biologists for measuring the orientation of single molecules in live cells is continually expanding. A recent review [8] identified three major categories of single molecule orientation determination techniques:

Spatial variation of emission techniques image single molecules and use the spatial distribution of intensity in the back focal plane [9] or in the image plane [10] to estimate their orientation. The best techniques in this category use defocusing or phase masks in the back focal plane to encode orientation and position information in the image [11]. These techniques can estimate the orientation of molecules in all orientations and only require a single frame, but they require complex reconstruction algorithms, expensive high numerical aperture (NA) optics, and sensitive detectors.

Spatial variation of illumination polarization techniques vary the polarization and intensity in the illumination path to excite molecules in specific orientations in the focal volume [12]. Although these techniques can accurately estimate the orientation of molecules in all orientations, they require scanning which makes these techniques too slow for live cell imaging.

Polarized illumination or detection techniques exploit the anisotropic absorption and emission pattern of single molecules to estimate their orientation. By measuring the total intensity in the detector plane while varying polarizer orientations on the illumination or detection path, the orientation of the molecule can be estimated. These techniques are easy to implement—changing the illumination or detection polarization is simple with a polarization splitter [4] or universal compensator [13]—and the reconstruction methods are straightforward [3, 4, 14]. The main drawback is that these techniques require several polarization frames to estimate the orientation of a single molecule. Despite the requirement for multiple frames, polarized illumination or detection methods are good choices for live cell imaging because of their good combination of speed and ease of implementation.

The choice remains—is it best to put polarizers on the illumination path or the detection path? Placing a polarizer in the illumination path lengthens acquisition time because the polarizer needs to be changed for each polarization frame, but polarized illumination provides the largest intensity differences between molecules in different orientations. Placing polarizers in the detection path doesn't slow down acquisition (multiple polarization frames can be collected at once with a polarization splitter), but polarized detection provides a smaller difference in intensity between molecules in different orientations than polarized illumination. We are most interested in finding the orientation of molecules with high precision, so polarized illumination is the method we consider and extend in this paper.

All single molecule orientation determination methods suffer from some degree of anisotropic orientation uncertainty, i.e., some molecular orientations cannot be determined as precisely as others. In some cases the orientation cannot be determined at all—the forward model can be degenerate for specific dipole orientations [14, 15]. We feel that the importance of isotropic orientation uncertainty has been underappreciated. To our knowledge, the only authors who have considered anisotropic orientation uncertainty have only analyzed a small set of molecular orientations instead of all orientations [11]. Our view is that an ideal technique for determining the orientation of single molecules can reconstruct the orientation with a small and nearly uniform uncertainty for all molecule orientations.

Recently, there has been increasing interest in multiview microscopy techniques for biological imaging [16–19]. Multiview microscopes offer two major advantages over single-view microscopes. First, multiview microscopes can achieve nearly isotropic resolution compared to the poor axial resolution of single-view microscopes. Second, multiview microscopes can use light-sheet illumination to reduce phototoxicity without requiring dedicated illumination optics. For example, if two orthogonal objectives are focused on the same point, then both objectives can alternate roles as the light-sheet illumination path and as the detection path. Light-sheet illumination offers a major reduction of phototoxicity because a light sheet only illuminates in focus regions while single-view microscopes illuminate out of focus regions. Together, these advantages make multiview microscopes good candidates for imaging live biological specimens for long periods.

In this work we explore the use of polarized illumination in multiview microscopes for determining the orientation of single molecules. Existing multiview microscopes can easily be outfitted with fast-switching polarizers that do not degrade image quality, so polarized illumination is a natural way to augment multiview microscopes for measuring the orientation of single molecules. Furthermore, multiview microscopes can achieve nearly isotropic resolution while delivering selective illumination. We hypothesize that multiview microscopes will also provide a small and uniform orientation uncertainty for single molecules in all orientations. In section 2 we develop the required theory for polarized illumination microscopy and develop information theoretic metrics to compare multiview microscopes. In section 3 we compare the results for a wide range of multiview microscope designs. Finally, in section 4 we discuss the results and their impact on polarized multiview microscope design.

2. Methods

In this section we develop a method to compare multiview polarized illumination microscopes for the task of reconstructing molecular orientations. In sections 2.1–2.4 we develop the forward model for single-frame microscopes with a fixed illumination and detection configuration. In section 2.5 we list a variety of ways that single-frame microscopes can be combined to create experimentally realizable multi-frame microscopes. Finally, in section 2.6 we develop metrics that we will use to compare multi-frame microscopes.

Note our distinction between a *frame* and a *view*. A frame refers to a single intensity measurement with a fixed polarizer setting, illumination path, and detection path. Acquiring additional frames entails varying the polarizer setting, illumination path, or detection path. A

view refers to a detection path, and multiview microscopes use multiple detection paths.

We use roman type for scalars, e.g., ϕ, θ ; bold lowercase type for vectors, e.g., $\mathbf{r}, \boldsymbol{\mu}$; hats for unit vectors, e.g., $\hat{\mathbf{r}}, \hat{\boldsymbol{\mu}}$; and bold capital type for matrices, e.g., \mathbf{R}, \mathbf{F} .

2.1. Absorption Efficiency

In this section we will calculate the *absorption efficiency* of a single molecule—the fraction of the incident power that is absorbed by the molecule. Our approach is inspired by Fourkas [14], but here we calculate the absorption efficiency instead of the detection efficiency.

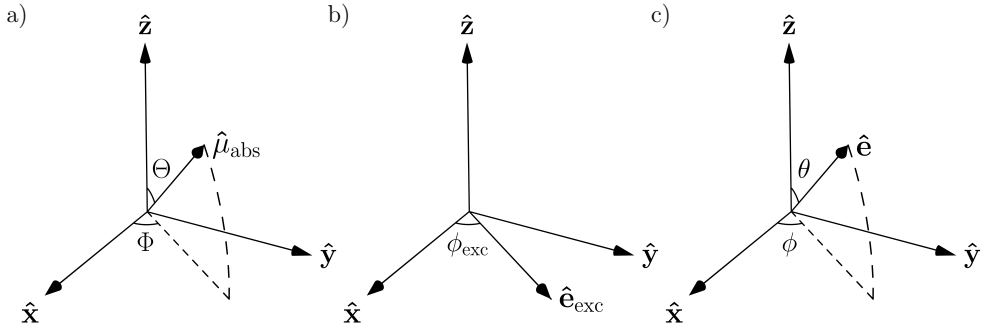


Fig. 1. Coordinate systems for a) the absorption dipole moment $\hat{\boldsymbol{\mu}}_{\text{abs}}$, b) the polarizer transmission axis $\hat{\mathbf{e}}_{\text{exc}}$, and c) the dummy integration vector $\hat{\mathbf{r}}$.

We consider a single molecule with an absorption dipole moment $\hat{\boldsymbol{\mu}}_{\text{abs}}$ that we express in spherical coordinates Θ and Φ (see Figure 1a)) as

$$\hat{\boldsymbol{\mu}}_{\text{abs}}(\Theta, \Phi) = \sin \Theta \cos \Phi \hat{\mathbf{x}} + \sin \Theta \sin \Phi \hat{\mathbf{y}} + \cos \Theta \hat{\mathbf{z}}. \quad (1)$$

We place the molecule at the focal point of an ideal, aplanatic, polarization-preserving objective with the optical axis aligned with the $\hat{\mathbf{z}}$ axis. Finally, we place a polarizer behind the objective with a variable transmission axis $\hat{\mathbf{e}}_{\text{exc}}$ that we express as

$$\hat{\mathbf{e}}_{\text{exc}}(\phi_{\text{exc}}) = \cos \phi_{\text{exc}} \hat{\mathbf{x}} + \sin \phi_{\text{exc}} \hat{\mathbf{y}}, \quad (2)$$

where ϕ_{exc} is the angle between the transmission axis of the polarizer and the positive $\hat{\mathbf{x}}$ axis (see Figure 1b)). We illuminate the polarizer with a beam of collimated light propagating along the optical axis, so the electric field incident on the objective is parallel with the transmission axis of the polarizer.

We denote the illuminated region of the objective by Ω . If we use unit vectors $\hat{\mathbf{r}}$ expressed in spherical coordinates θ and ϕ (see Figure 1c)) as

$$\hat{\mathbf{r}}(\theta, \phi) = \sin \theta \cos \phi \hat{\mathbf{x}} + \sin \theta \sin \phi \hat{\mathbf{y}} + \cos \theta \hat{\mathbf{z}}, \quad (3)$$

then the region Ω can be expressed as

$$\Omega = \{\phi, \theta \mid 0 < \phi \leq 2\pi, 0 < \theta \leq \alpha\}, \quad (4)$$

where α is the angle between the optical axis and the most oblique illuminating ray. Equivalently, α can be expressed in terms of NA using

$$\text{NA} = n \sin \alpha, \quad (5)$$

where n is the index of refraction of the sample medium. Note that the NA of the objective is always greater than or equal to the illumination NA because we can under fill the back aperture of the objective.

The objective focuses the collimated illumination by applying a position-dependent rotation to the electric field which we model by multiplying the incident electric field $\hat{\mathbf{e}}$ by a position-dependent rotation matrix

$$\mathbf{R}(\hat{\mathbf{r}}) = \begin{bmatrix} \cos \theta \cos^2 \phi + \sin^2 \phi & (\cos \theta - 1) \sin \phi \cos \phi & -\sin \theta \cos \phi \\ (\cos \theta - 1) \sin \phi \cos \phi & \cos \theta \sin^2 \phi + \cos^2 \phi & -\sin \theta \sin \phi \\ \sin \theta \cos \phi & \sin \theta \sin \phi & \cos \theta \end{bmatrix}. \quad (6)$$

To find the absorption efficiency η_{abs} of a single molecule if it were illuminated by a single ray, we take the unit incident electric field $\hat{\mathbf{e}}$, take the dot product with the absorption dipole moment, then take the modulus squared

$$\eta_{\text{abs}} = |\hat{\mu}_{\text{abs}} \cdot \hat{\mathbf{e}}_{\text{exc}}|^2. \quad (7)$$

To find the absorption efficiency of a single molecule under incoherent focused light, we integrate over all rays and divide by the total incident power which gives the vector expression

$$\eta_{\text{abs}} = \frac{\int_{\Omega} d\hat{\mathbf{r}} |\hat{\mu}_{\text{abs}} \cdot \mathbf{R}(\hat{\mathbf{r}}) \hat{\mathbf{e}}_{\text{exc}}|^2}{\int_{\Omega} d\hat{\mathbf{r}}}. \quad (8)$$

We substitute equations 1–6 into equation 8, evaluate the integrals, and simplify to express the absorption efficiency in scalar notation as

$$\eta_{\text{abs}} = D \{ A + B \sin^2 \Theta + C \sin^2 \Theta \cos [2(\Phi - \phi_{\text{exc}})] \} \quad (9)$$

where

$$A = \frac{1}{4} - \frac{3}{8} \cos \alpha + \frac{1}{8} \cos^3 \alpha \quad (10a)$$

$$B = \frac{3}{16} \cos \alpha - \frac{3}{16} \cos^3 \alpha \quad (10b)$$

$$C = \frac{7}{32} - \frac{3}{32} \cos \alpha - \frac{3}{32} \cos^2 \alpha - \frac{1}{32} \cos^3 \alpha \quad (10c)$$

$$D = \frac{4}{3(1 - \cos \alpha)}. \quad (10d)$$

At the beginning of this section we assumed that the molecule was located at the focal point of the condenser. If the illumination objective is aplanatic and we use Köhler illumination, then we can relax this assumption and the above expressions are valid for molecules anywhere in the focal plane.

We also assumed that we used incoherent illumination, but we can extend these results to light-sheet illumination that uses a scanned coherent laser. If we illuminate the back aperture with a weakly focused laser beam and scan the laser beam slowly—if the scan velocity is much less than the beam waist radius divided by the coherence time—we can ignore longitudinal excitation and the molecule will be excited as if a single plane wave was incident. Therefore, we can find the absorption efficiency of a molecule under weakly focused scanned laser illumination by taking the limit of equation 9 as $\alpha \rightarrow 0$ (or by plugging equation 1 and 2 into equation 7) giving

$$\eta_{\text{abs}} = \sin^2 \Theta \cos^2(\Phi - \phi_{\text{exc}}), \quad (11)$$

which is recognizable as Malus' law generalized to three dimensions. This means that light-sheet illumination is approximately equivalent to widefield illumination with a low NA. Notice that the absorption efficiency can take its maximum range of values ($\eta_{\text{abs}} \in [0, 1]$) when $\alpha = 0$.

2.2. Detection Efficiency

Fourkas calculated the detection efficiency of a single molecule when an objective with a polarizer is aligned along the $\hat{\mathbf{z}}$ axis [14]. We use his expressions to calculate the detection efficiency without a polarizer as

$$\eta_{\text{det}} = 2(A + B \sin^2 \Theta). \quad (12)$$

The detection efficiency only depends on Θ , not Φ , because there is no detection polarizer. We have assumed that the absorption dipole moment is equal to the emission dipole moment.

Note that A and B in equation 10 are a factor of $\frac{3}{2}$ larger than the expressions given by Fourkas. We found that Fourkas' expressions were incorrectly normalized (the limit of η_{det} as $\alpha \rightarrow \pi/2$ should be 1), and the extra factor of $\frac{3}{2}$ corrects the error. This correction does not affect Fourkas' orientation reconstruction but it does mean that Fourkas' algorithm under predicts the total emitted intensity by a factor of $\frac{3}{2}$.

Also note that the detection efficiency can take its maximum range of values when B takes its maximum value, i.e. when $\alpha = \arccos\left(\frac{1}{\sqrt{3}}\right) \approx 54.7^\circ$.

2.3. Oblique Illumination and Detection

In sections 2.1 and 2.2 we assumed that both the illumination and detection objectives had $\hat{\mathbf{z}}$ aligned optical axes, i.e., the same objective was used for illumination and detection. To extend the forward model to oblique optical axes which allows for non-coincident illumination and detection objectives, we express the dipole orientation in rotated coordinates using the following expressions

$$\Theta' = \arccos(\sin \psi \cos \Phi \sin \Theta + \cos \psi \cos \Theta) \quad (13)$$

$$\Phi' = \begin{cases} \arccos\left(\frac{\cos \psi \cos \Phi \sin \Theta - \sin \psi \cos \Theta}{\sqrt{1 - (\sin \psi \cos \Phi \sin \Theta + \cos \psi \cos \Theta)^2}}\right) & 0 \leq \Phi < \pi \\ -\arccos\left(\frac{\cos \psi \cos \Phi \sin \Theta - \sin \psi \cos \Theta}{\sqrt{1 - (\sin \psi \cos \Phi \sin \Theta + \cos \psi \cos \Theta)^2}}\right) & -\pi \leq \Phi < 0 \end{cases} \quad (14)$$

where ψ is the angle of a right handed rotation about the $\hat{\mathbf{y}}$ axis that maps the $\hat{\mathbf{z}}$ axis onto the new optical axis.

2.4. Single-Frame Microscopes

The detected intensity is the product of the sample exposure I_{tot} , the absorption efficiency, and the detection efficiency

$$I = I_{\text{tot}} \eta_{\text{abs}} \eta_{\text{det}}. \quad (15)$$

Equation 15 is the forward model for a *single-frame microscope*. Figure 2 shows the efficiencies from three representative examples of single-frame microscopes.

The intensity measured by a single-frame microscope does not give us enough information to reconstruct the orientation of a single molecule. Next, we will consider combining several single-frame microscopes to create *multi-frame microscopes*.

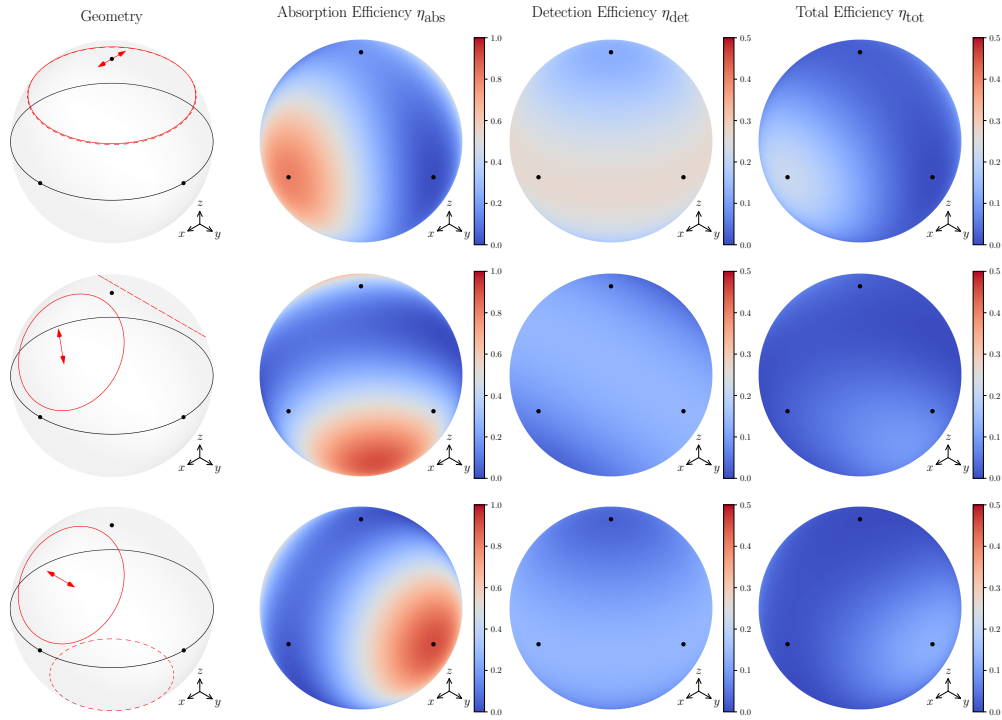


Fig. 2. Representative examples of single-frame microscopes.

Columns left to right: 1) schematics of single-frame microscopes where the solid line encloses the illumination solid angle, the dashed line encloses the detection solid angle, and the arrow indicates the transmission axis of the illumination polarizer; 2) the absorption efficiency, see equation 9; 3) the detection efficiency, see equation 12; (4) the total efficiency, the product of the absorption and detection efficiencies.

Rows top to bottom: 1) coincident illumination ($NA = 1.1$ with x -polarized light) and detection ($NA = 1.1$); 2) non-coincident orthogonal illumination ($NA = 0.8$) and detection ($NA = 0.8$); 3) non-coincident 135° -separated illumination ($NA = 0.8$) and detection ($NA = 0.8$). All simulations use $n = 1.33$.

2.5. Multi-Frame Microscopes

One way to collect multiple frames is to add a universal compensator to the illumination arm and rapidly select the incident polarization by changing ϕ_{exc} [13]. All of the multi-frame microscopes we will consider in this paper use four frames per view with the illumination polarization separated by 45° .

We also consider several dual-view designs. We evaluate two-view designs that allow for illumination and detection from both objectives (see [16] for a dual-view design). In all cases we consider the effect of varying the illumination and detection numerical aperture. We also consider asymmetric NA designs (see [19] for an asymmetric NA design) and the effect of asymmetric sample exposures. Note that we use the word *symmetry* to refer to dual-view designs with objectives that are identical and the word *asymmetry* to refer to dual-view designs with objectives that have a different NA or sample exposure.

All multiview microscopes are subject to steric constraints—the objectives must not collide

with the cover slip or each other. We only consider microscope designs that meet these criteria.

2.6. Evaluation Metrics

Our goal is to evaluate the ability of a microscope design to estimate the orientation of a single molecule (via parameters Θ and Φ) from intensity data.

A common way to evaluate the ability to estimate the parameters Θ and Φ from the data is to calculate the Cramer-Rao lower bound (CRLB) for each parameter [20]. The CRLBs are given by the diagonal elements of the inverse of the Fisher information matrix, and they give the minimum variance of an unbiased estimator for each parameter. For each microscope design and molecule orientation we calculate the Fisher information matrix. If the intensity is Poisson distributed the Fisher information matrix is given by

$$\mathbf{F} = \sum_{k=1}^N \frac{1}{I_k} \begin{bmatrix} \frac{\partial I_k}{\partial \Theta} \frac{\partial I_k}{\partial \Theta} & \frac{\partial I_k}{\partial \Theta} \frac{\partial I_k}{\partial \Phi} \\ \frac{\partial I_k}{\partial \Phi} \frac{\partial I_k}{\partial \Theta} & \frac{\partial I_k}{\partial \Phi} \frac{\partial I_k}{\partial \Phi} \end{bmatrix} \quad (16)$$

where I_k is the intensity measured in the k th frame of an N -frame microscope. Agrawal et al. used the square root of the product of the CRLBs multiplied by the Jacobian determinant, $\sin \Theta \sqrt{\mathbf{F}_{0,0}^{-1} \mathbf{F}_{1,1}^{-1}}$, to find the area of uncertainty in parameter space [11].

CRLBs and the associated area of uncertainty are parametrization dependent, i.e., if we choose a different coordinate system these metrics will change. We would like to compare microscope designs without choosing a parametrization, so instead we use

$$\sigma_\Omega \equiv \sin \Theta \sqrt{\det\{\mathbf{F}^{-1}\}} \quad (17)$$

as our evaluation metric. We calculate the determinant of the inverse Fisher information matrix—a parametrization-independent value called the *generalized variance* [21]—take the square root, then multiply by the Jacobian determinant, $\sin \Theta$. We call σ_Ω the *solid-angle uncertainty* because it has units of steradians and is a parametrization independent measure of the orientation uncertainty.

For each multi-frame microscope we calculate σ_Ω at 10,000 approximately equally spaced points on the unit sphere. A desirable microscope design will have a small solid-angle uncertainty that is uniform for all molecule orientations. The most straightforward way to find the location and scale of the solid-angle uncertainty is to use the mean and variance, respectively. However, because the solid-angle uncertainty admits extremely large values that can change the mean and variance dramatically depending on the sample points, we use the median and median absolute deviation (MAD)—the median of the data's absolute difference from the median—as robust alternatives to the mean and variance.

To compare multi-frame microscopes with different numbers of frames fairly, we kept the total exposure to the sample constant by choosing $I_{\text{tot}} = \frac{4000}{N}$. Note that I_{tot} is a measure of exposure to the sample, not the detected intensity or the total intensity emitted by the molecule.

3. Results

Figure 3 shows our results for single-view designs where a single objective is used for illumination and detection. We swept through the illumination and detection NA while keeping the sample exposure constant, and we found that the lowest median and MAD of the solid-angle uncertainty occurs with a small illumination NA and a large detection NA where $\alpha \approx 57.4^\circ$. A small illumination NA maximizes the range of absorption efficiencies, while a large detection NA maximizes the number of detected photons and the range of the detection efficiencies. Note

the relative importance of illumination and detection NAs—reducing the illumination NA (an inexpensive modification requiring under filling the back aperture) improves the solid angle uncertainty much less than increasing the detection NA (an expensive modification requiring a higher NA objective). Also note in Figure 3b) that single-view designs suffer from high orientation uncertainty when the molecules are oriented along the optical axis (the molecules are not efficiently excited), near the transverse plane (it is ambiguous whether the molecule is oriented above or below the transverse plane), and near the polarizer orientations (it is ambiguous whether the molecule is on either side of the polarizer orientation).

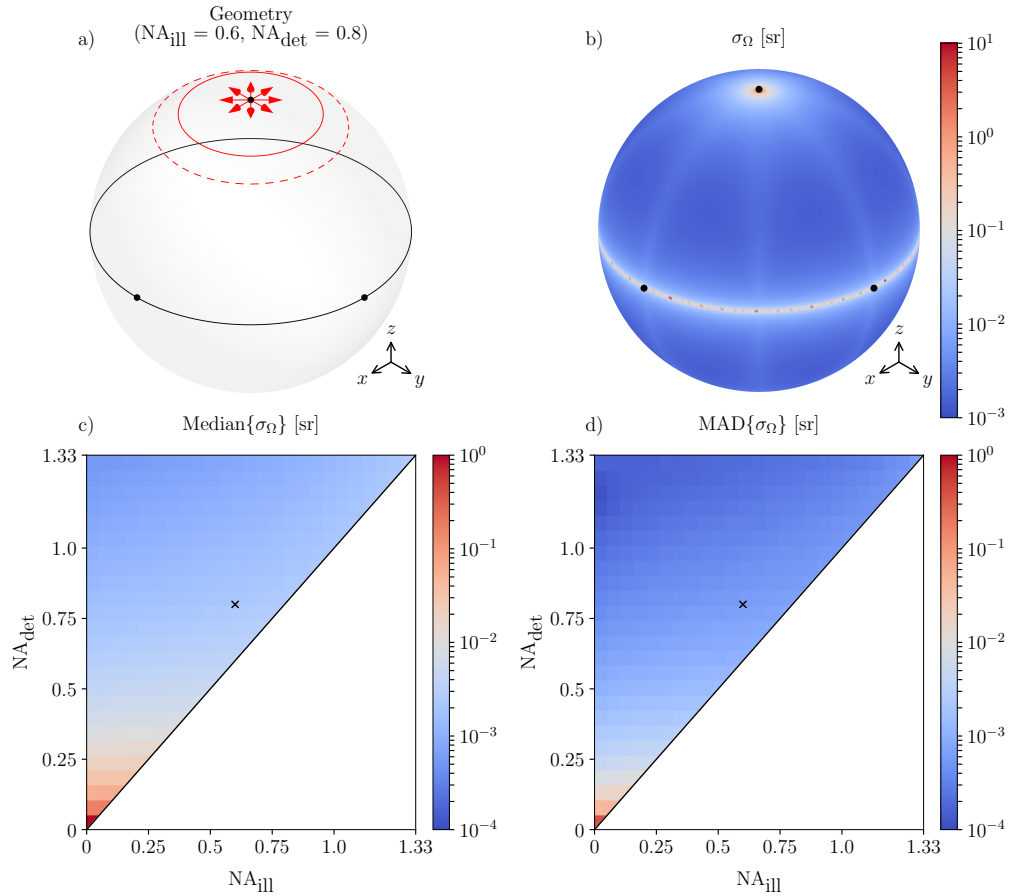


Fig. 3. Single-view microscope with varying illumination and detection NA. a) Schematic of a single-arm four-frame epi-illumination microscope. The red arrows indicate the four illumination polarization orientations—one for each frame. b) Solid angle uncertainty for the microscope in a). c) Median of the solid-angle uncertainty as a function of illumination and detection NA. d) MAD of the solid-angle uncertainty as a function of illumination and detection NA. The microscope in a) and b) is indicated by a cross in c) and d).

Figures 4 and 5 show our results for dual-view symmetric widefield designs. We illuminate from one objective and detect from the other for four polarization frames, then we repeat the polarization frames with the same objectives in reversed roles. In Figure 4 we sweep through the NA of both objectives and the angle between the objectives while considering steric constraints. Note how adding a second view removes the high uncertainty region in the transverse plane. The

dual-view microscope still has high uncertainty regions near the optical axes, but the uncertainty is reduced by almost two orders of magnitude compared to the single-view microscope. We find that the lowest median of the solid-angle uncertainty occurs with the largest possible NA objectives. We also find that increasing NA always lowers the MAD, but orthogonal arms are not always best. At large NA, it is advantageous to move the objectives together or against the cover slip. Given the high uncertainty in the transverse plane for a single-view shown in Figure 3b), we can see why oblique views perform better than orthogonal views—oblique views are complementary because the regions of high orientation uncertainty from each view do not overlap.

Figure 5 shows our results when we used a dual-view symmetric orthogonal widefield design and varied the illumination and detection NA. Our results are similar to the single-view case in Figure 3. We find that the best designs use a small illumination NA (like light-sheet illumination) and a large detection NA where $\alpha \approx 57.4^\circ$. This means that dual-view light-sheet illumination geometries are an excellent choice for uniformly reconstructing the orientation of single molecules.

Figure 6 shows our results for dual-view asymmetric light-sheet illumination designs. We used light-sheet illumination on both sides and kept the objectives orthogonal so that the light sheet from one objective illuminates the focal plane of the other objective. We made the objectives as large as possible so that both objectives would touch the cover slip and each other ($\alpha_1 + \alpha_2 = 90$ in Figure 6a)). We swept through the NA asymmetry and the sample exposure asymmetry while keeping the total sample exposure constant, and found that symmetric designs are at a local minimum of the median and MAD of the solid-angle uncertainty. We also found that at extreme asymmetries where the exposure from the low NA arm is much larger than the exposure from the high NA arm (top-left and bottom-right corners of Figures 6c) and d)) the median and MAD are comparable to the symmetric light-sheet microscope. This means that if a very high NA objective is available and a low NA objective can provide light sheet illumination, this microscope will perform comparably with a dual-view microscope with two objectives of medium NA. Figure 6 also shows that designs with slightly asymmetric NA can trade off a low solid-angle uncertainty median for a low solid-angle uncertainty MAD by changing the sample exposure ratio.

Table 1 shows a summary of our evaluation metrics for the best microscopes in each class. The single-view widefield microscope with a large illumination NA and high detection NA has the lowest solid-angle uncertainty median but the largest max. The dual-view oblique symmetric widefield with an intermediate NA performs reasonably well on all three metrics, while the dual-view orthogonal symmetric light sheet with the largest possible detection NA performs very well on all three metrics.

Table 1. Comparison of the best designs in each class of microscope. All values are in steradians.

Microscope Type	Max{ σ_Ω }	Median{ σ_Ω }	MAD{ σ_Ω }
Single-view widefield ($NA_{\text{ill}}=0$, $NA_{\text{det}}=1.1$)	3.04×10^0	8.20×10^{-4}	1.40×10^{-4}
Dual-view oblique symmetric widefield ($NA=0.6$, $\beta=53^\circ$)	1.35×10^{-1}	4.49×10^{-3}	9.17×10^{-4}
Dual-view orthogonal symmetric light-sheet ($NA=0.94$)	3.13×10^{-3}	1.28×10^{-3}	1.14×10^{-4}

4. Discussion and Conclusions

In this work we have developed a model to predict the intensities measured by polarized illumination microscopes in a wide range of geometries, developed metrics to measure the ability of a microscope design to estimate the orientation of single molecules, and used these metrics to compare a wide range of microscope designs. Our main result is a short list of design heuristics that can be used to design polarized-illumination single-molecule orientation microscopes:

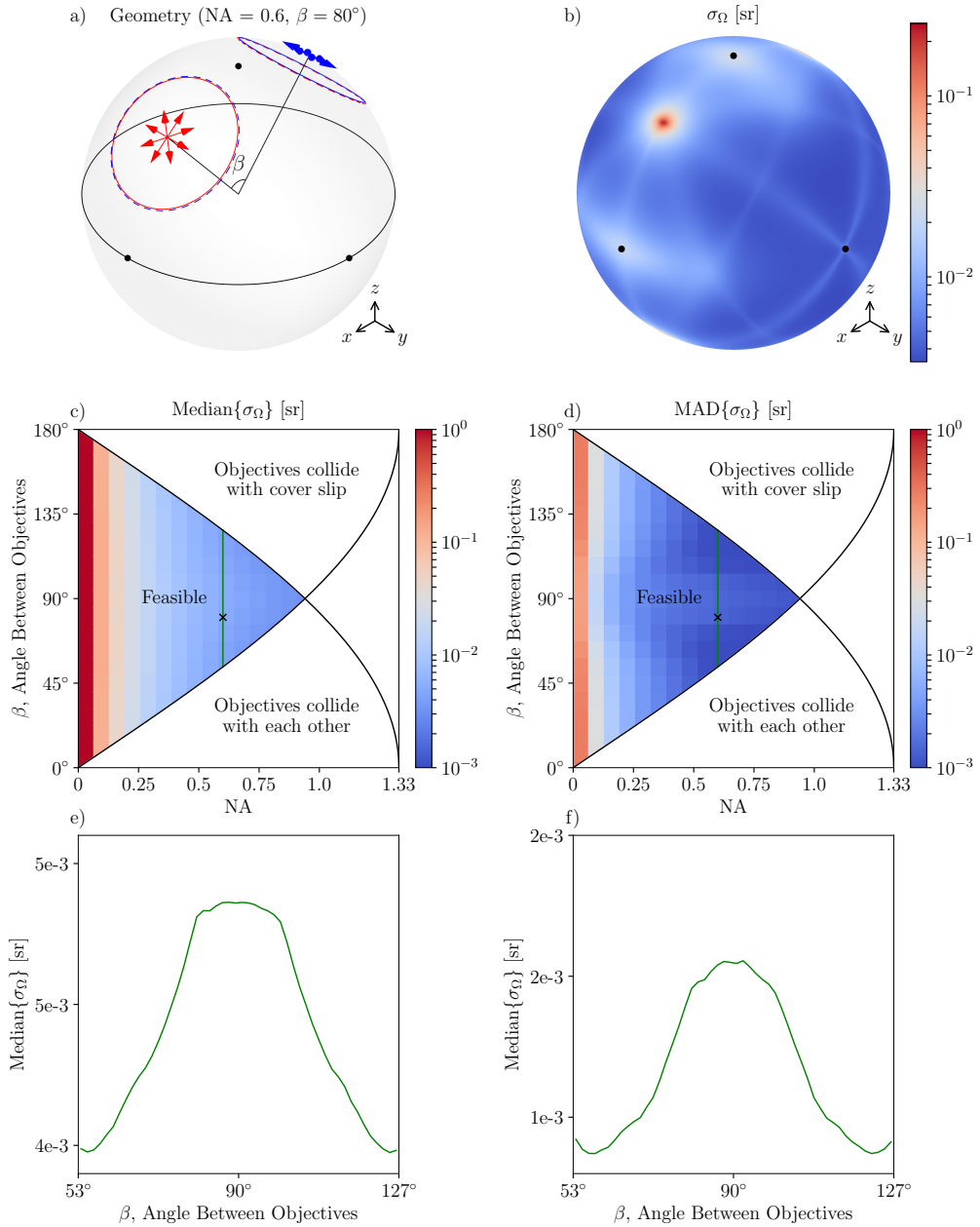


Fig. 4. Dual-view symmetric widefield designs with varying NA and angle between objectives.
 a) Schematic of the microscope. We illuminate with the first objective (red solid) and detect from the second objective (red dashed). Then we illuminate from the second objective (blue solid) and detect from the first objective (blue dashed). b) Solid angle uncertainty for the microscope in a). c) Median of the solid-angle uncertainty as a function of NA and the angle between the objectives. d) MAD of the solid-angle uncertainty as a function of NA and the angle between the objectives. The microscope in a) and b) is indicated by a cross in c) and d). e) Median of the solid-angle uncertainty as a function of the angle between the objectives when NA=0.6. f) MAD of the solid-angle uncertainty as a function of the angle between the objectives when NA=0.6. The profile in e) and f) is taken along the green line in c) and d).

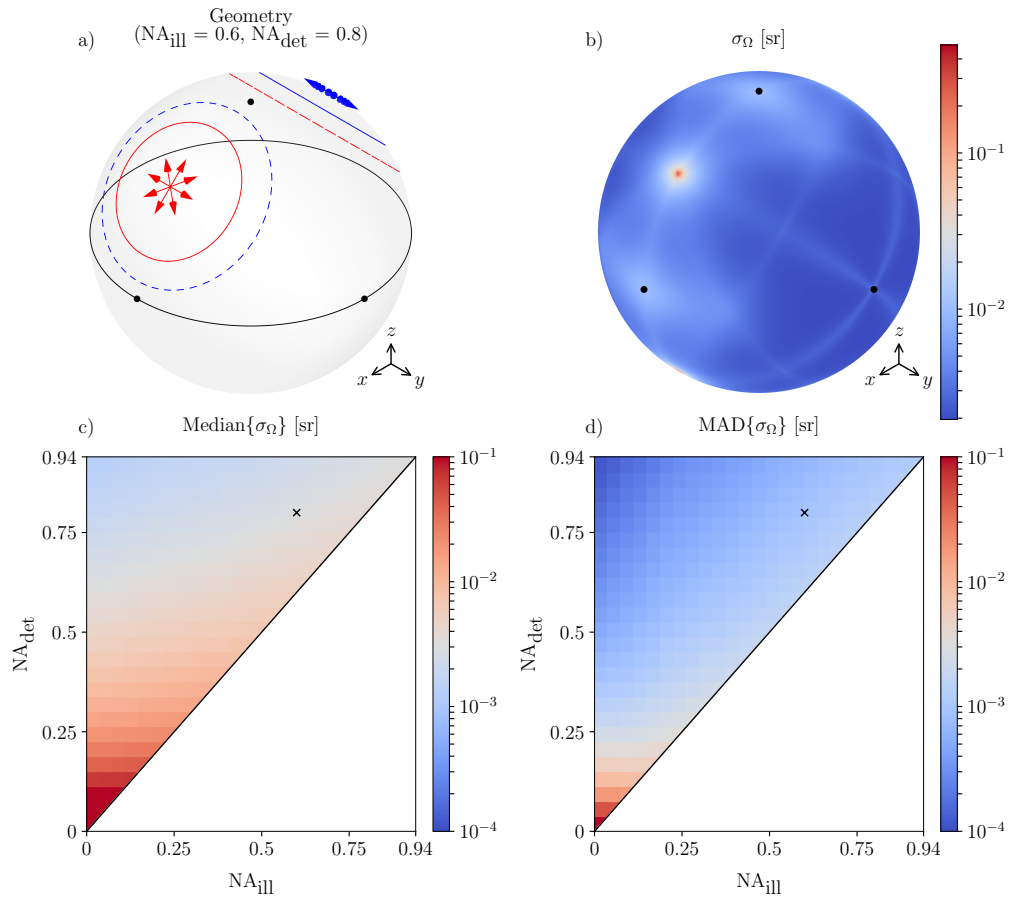


Fig. 5. Dual-view symmetric orthogonal widefield designs with varying illumination and detection NA. a) Schematic of the microscope. b) Solid angle uncertainty for the microscope in a). c) Median of the solid-angle uncertainty as a function of illumination and detection NA. d) MAD of the solid-angle uncertainty as a function of illumination and detection NA. The microscope in a) and b) is indicated by a cross in c) and d).

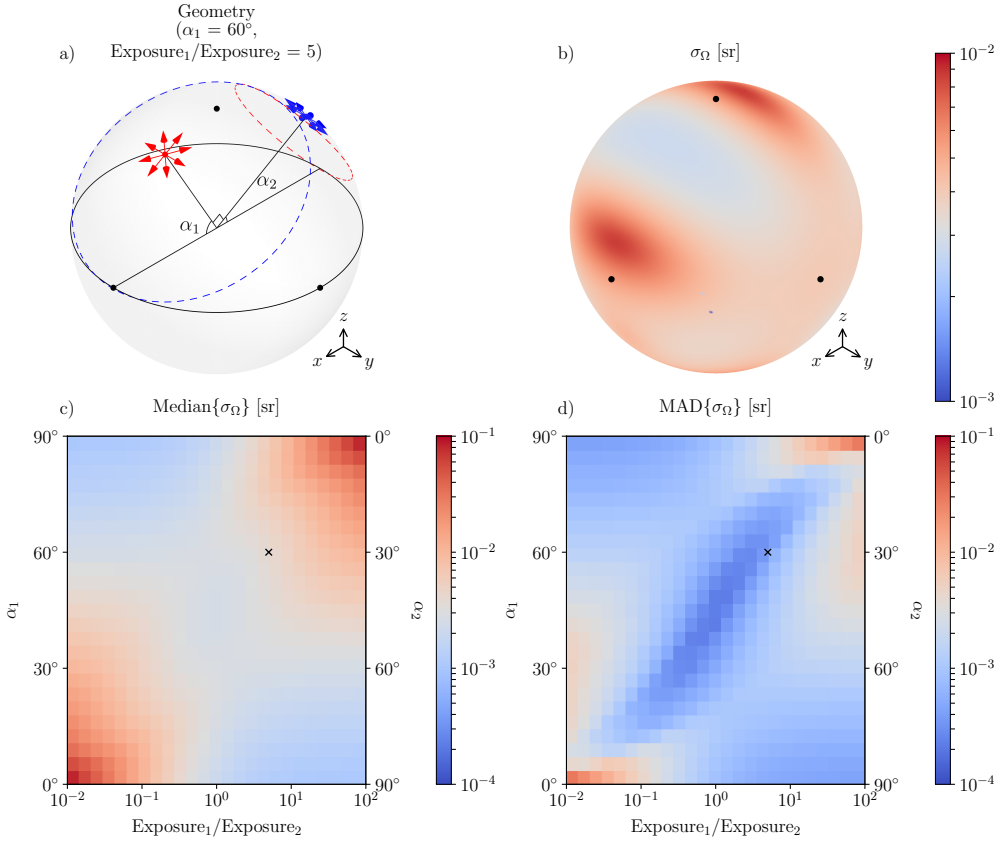


Fig. 6. Dual-view asymmetric light-sheet illumination designs with varying NA and sample exposure asymmetry. a) Schematic of the microscope. b) Solid angle uncertainty for the microscope in a). c) Median of the solid-angle uncertainty as a function of NA and sample exposure asymmetry. d) MAD of the solid-angle uncertainty as a function of NA and sample exposure asymmetry. The microscope in a) and b) is indicated by a cross in c) and d).

- All microscopes benefit from a small illumination NA and a large detection NA with $\alpha \approx 57.4^\circ$.
- Dual-view microscopes outperform single-view microscopes, and dual-view microscopes remove the high uncertainty region in the transverse plane of single-view microscopes.
- High NA dual-view widefield microscopes are best when the two views are oblique. Oblique views are complementary because their high uncertainty transverse planes do not overlap.
- Symmetric NA dual-view orthogonal light-sheet microscopes provide a good compromise between cost, solid-angle uncertainty median, and solid-angle uncertainty MAD. Asymmetric NA dual-view orthogonal light-sheet microscopes can improve the solid-angle uncertainty median or MAD by changing the sample exposure ratio between the two views.

Our results are limited in several ways. First, we only consider single molecules in homogeneous environments. We ignore light reflected from the cover slip and any other inhomogeneities in

the sample. If we considered light reflected from the cover slip we expect that the results would put a lower weighting on large detection NAs because we would collect more light. Second, we only considered ideal, polarization preserving, aplanatic objectives. In practice, these conditions are not always satisfied and the power from high NA rays is apodized by a factor of $\frac{n}{\cos \Theta}$ [22]. Therefore, our results are most accurate for low NA rays and get progressively worse for high NA rays, although our major conclusions would not change if we included this apodization factor. The main advantage of ignoring apodization is the tractability of the problem—we have provided approximate closed-form solutions for the illumination and detection efficiencies that have allowed us to draw useful design conclusions.

To compare the microscopes in this paper we used a fixed sample exposure. We think that this is the fairest way to compare microscopes with different numbers of frames. However, in cases where sample exposure and time are not an issue it may be more useful to compare microscopes with the same detection exposure per frame. This comparison would favor multiple frame microscopes even more than the results in this paper, because equal detection exposure per frame would improve photon counting statistics.

We have considered single- and dual-view microscopes in a variety of cases, but more multiview microscopes can be analyzed with the framework we have developed. Wu et. al. have developed a three-view design with a third objective below the cover slip [18]. Light-field detection schemes are also a type of multiview microscope [23], and we plan to extend our analysis to this case in future work.

Although we have only considered single-molecule orientation determination in this work, polarized illumination techniques can be applied to find the distribution of ensembles of molecules [3,4]. In future work we will investigate the ability of multiview polarized illumination microscopes to estimate the orientation and distribution of ensembles of molecules.

We have only considered polarized illumination. In the introduction we discussed why we prefer polarized illumination to polarized detection, but there is information to be gained by adding polarized detection to the techniques discussed in this paper. Adding a polarization splitter to the detection arm can increase the information available for reconstructing the orientation of a single molecule without increasing the acquisition time.

We conclude that multiview microscopes are useful tools for determining the orientation of single molecules. Using simple design heuristics, we can design polarized illumination multiview microscopes that can determine the orientation of single molecules with a small and uniform orientation uncertainty.

Funding

TODO

Disclosures

The authors declare that there are no conflicts of interest related to this article.